

# Spin relaxation of conduction electrons in coupled quantum wells

C. A. Bravo-Velázquez<sup>✉,\*</sup>, L.F. Lastras-Martínez,<sup>†</sup> O. Ruiz-Cigarrillo<sup>✉</sup>, G. Flores-Rangel<sup>✉</sup>, and L. E. Tapia-Rodríguez<sup>✉</sup>  
*Instituto de Investigación en Comunicación Óptica, Universidad Autónoma de San Luis Potosí Alvaro Obregón 64,  
 78000 San Luis Potosí, S.L.P., México*

K. Biermann<sup>✉</sup> and P. V. Santos<sup>‡</sup>

*Paul-Drude-Institut für Festkörperelektronik, Leibniz-Institut im Forschungsverbund Berlin e.V., Hausvogteiplatz 5-7, 10117, Germany*



(Received 22 February 2023; revised 26 May 2023; accepted 10 July 2023; published 18 July 2023)

The spin of the conduction-band electrons in a quantum well constitutes a promising two-level system for realizing a quantum bit in the solid state. One of the important parameters in the spin dynamics is their relaxation time. It is desired to develop models and semiconductor structures in order to control it. There are several reported examples of spin lifetime control in quantum wells. Double quantum wells in a semiconductor heterostructure allow the modulation of the relaxation time. By changing the relative thicknesses of the wells in the double quantum well system, the wave function for the lowest-energy level of the conduction band can be distributed symmetrically or asymmetrically with respect to the coupling barrier between the quantum wells to control the Dresselhaus and Rashba components of the spin-orbit coupling and, consequently, the relaxation time. To detect and characterize this effect, circularly polarized photoluminescence was used at low temperatures (19 K). The results reported in the present paper suggest that this coupled double quantum well system enables the design of structures that allows for the control of the relaxation time and the performance of the electron spin as a quantum bit.

DOI: [10.1103/PhysRevB.108.045306](https://doi.org/10.1103/PhysRevB.108.045306)

## I. INTRODUCTION

Spin dynamics and its related phenomena in semiconductors have attracted a lot of attention in recent years due to their potential applications in devices [1–4] and quantum computing [1,2]. The manipulation of the spin of free carriers is of fundamental importance in the development of the spintronics field [2].

The spin-orbit coupling (SOC) of carriers plays an important role in the spin dynamics and, in particular, in the spin relaxation time. SOC induces a spin-dependent energy splitting of the bands due to an effective magnetic field that depends on the quasimomentum  $\mathbf{k}$  of the carriers. Two mechanisms that induce spin splitting are considered, the Dresselhaus and the Rashba effects [5]. For intrinsic semiconductors without inversion symmetry, such as zinc-blende crystals ( $T_d$  symmetry), the spin splitting is associated with the Dresselhaus effect [6,7]. If the symmetry is reduced from  $T_d$  to  $C_{2v}$ , additionally to the Dresselhaus effect, a Rashba effect contributes to the spin splitting. This occurs if an electric field is applied perpendicularly to the (001) surface or for asymmetric quantum wells (QWs) [8–11]. In the later case, the asymmetry can be obtained with barriers of different heights [10,11] with different chemical compositions [12] or by triangular barriers [8], for instance.

Double quantum well (DQW) systems constitute an excellent platform to study interactions between confined

energy-level transport and spin dynamics [13]. These structures consist of two coupled QWs separated by a thin barrier. By changing the relative thicknesses of the QWs, it is possible to modulate the asymmetry of the system [14] and, thus, to modify the spin dynamics by changing the relative strength of the Dresselhaus and Rashba contributions to the SOC [15].

To study the spin dynamics in DQWs, we have used polarization-resolved photoluminescence (PL) spectroscopy excited with left- ( $\sigma^-$ ) or right- ( $\sigma^+$ ) circularly polarized laser beams. Figure 1 compares a simplified energy diagram for the conduction and valence bands of a QW or a DQW system [16]. Due to quantum confinement, heavy- and light-hole levels lift their degeneracy. Under this condition, by exciting with  $\sigma^+$  polarization [Fig. 1(a)] with an energy larger than the energy between conduction and light holes bands, the transitions  $-3/2 \rightarrow -1/2$  and  $-1/2 \rightarrow +1/2$  are excited with intensities  $I \propto 3/4$  and  $I \propto 1/4$ , respectively [16]. The PL spectrum comprises, in general, components with  $\sigma^+$  and  $\sigma^-$  polarization [Fig. 1(b)]. It is important to note that holes were considered completely depolarized before recombination [17]. The degree of circular polarization of the PL is defined as  $\mathcal{P} = (I^{\sigma^+} - I^{\sigma^-}) / (I^{\sigma^+} + I^{\sigma^-})$  and has a maximum value of  $\mathcal{P}_o = 0.5$  [16].

Taking into account the electron spin-relaxation time  $\tau_s$  and the recombination lifetime  $\tau$ , the degree of circular polarization of the PL can be written as [18]

$$\mathcal{P} = \mathcal{P}_o / (1 + \tau / \tau_s), \quad (1)$$

where  $\tau$  and  $\tau_s$  are the recombination and spin lifetimes, respectively. In the limits  $\tau_s \ll \tau$  and  $\tau_s \gg \tau$ ,  $\mathcal{P}$  tends to zero and  $\mathcal{P}_o$ , respectively. We demonstrate in the present paper,

\*c.a.bravovelazquez@gmail.com

<sup>†</sup>lflm@cactus.iico.uaslp.mx; gdarbel@prodigy.net.mx

<sup>‡</sup>santos@pdi-berlin.de

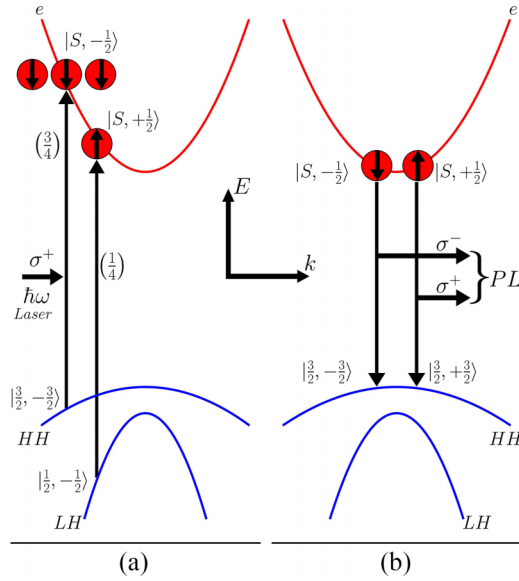


FIG. 1. Energy band diagrams of a QW. (a) The circularly polarized laser (indicated by  $\sigma^+$  in the figure) is absorbed with strengths of  $3/4$  and  $1/4$  for the electron-heavy hole (HH)  $|3/2 - 3/2\rangle$  and electron-light hole (LH)  $|3/2 - 1/2\rangle$  transitions, respectively. (b) The PL spectrum comprises  $\sigma^+$  and  $\sigma^-$  components. The polarization degree of the PL reach the maximum value of  $\mathcal{P}_o = 0.5$  for the electron-HH transition (see the text for details).

that  $\tau_s$  can be controlled in a DQW systems by changing the relative thicknesses of the QWs and determining  $\mathcal{P}$  by means of PL measurements.

## II. EXPERIMENTAL RESULTS

The experiments were performed on (001)-oriented GaAs QWs with the following layer structure: GaAs(10 nm)/Al<sub>0.15</sub>Ga<sub>0.85</sub>As(300 nm)/QW<sub>1</sub>(d)/Al<sub>0.15</sub>Ga<sub>0.85</sub>As(2.0 nm)/QW<sub>2</sub>(11.9 nm)/Al<sub>0.15</sub>Ga<sub>0.85</sub>As(300 nm)/n-Al<sub>0.15</sub>Ga<sub>0.85</sub>As(600 nm)/GaAs substrate. Three samples with the following thicknesses for QW<sub>1</sub> were measured: (a)  $d = 11.9$  nm (42 ML), where ML represents monolayer, (b)  $d = 13.8$  nm (49 ML), and (c)  $d = 23.7$  nm (84 ML). The structure of the first sample is symmetric, and the others are asymmetric.

PL experiments were carried out under excitation by a semiconductor laser with a wavelength of  $\lambda = 787$  nm and a power density of  $I = 0.8$  mW/mm<sup>2</sup>. By using a  $\lambda/4$  plate and a liquid-crystal half-wave variable retarder in tandem, the polarization of the laser can be switched between left- and right-circular polarizations. The laser is incident normal to the surface of the sample and focused within a spot size of 500  $\mu$ m of diameter. The PL is directed to a linear polarizer prism to select the left- and right-circular polarizations by rotating the prism. The sample is chilled at cryogenic temperatures (19 K) by means of a low-vibration helium closed-cycle cryocooler. The PL signal is collected and detected by using an imaging spectrometer with a resolution of 0.025 nm equipped with a thermoelectric-cooled camera as the detector. The systematic polarization errors of our PL system was estimated by measuring the degree of circular polarization  $\mathcal{P}$ , for the reflectance

(in the range from 800 to 830 nm) for a flat mirror and for the sample at room temperature. Assuming that in a perfect system  $\mathcal{P} = 1$  in both cases, we estimate from the experiments an error of approximately  $\pm 0.002$  in our  $\mathcal{P}$  measurements.

Figure 2 shows PL spectra for QW<sub>1</sub> thicknesses of (a)  $d = 11.9$  nm, (b)  $d = 13.8$  nm, and (c)  $d = 23.7$  nm. In this case, the excitation laser is  $\sigma^+$  circularly polarized. The blue and the red PL spectra, correspond to the  $\sigma^+$  (cross-) and  $\sigma^-$  (co-) circular polarized with respect to the excitation polarization, respectively. For the heavy-hole transitions (HH in Fig. 2) the PL intensity of the  $\sigma^-$  polarization is stronger than of the  $\sigma^+$ , whereas, for the light-hole transitions (LH in Fig. 2) this relation is the opposite. This behavior is expected considering that heavy-hole transitions  $-1/2 \rightarrow -3/2$  and  $+1/2 \rightarrow +3/2$  produce PL with polarization  $\sigma^-$  and  $\sigma^+$ , respectively, whereas, for the light-hole transitions  $-1/2 \rightarrow +1/2$  and  $+1/2 \rightarrow -1/2$  produce PL with polarizations  $\sigma^+$  and  $\sigma^-$ , respectively. Thus, the degree of circular polarization has opposite signs for the HH and LH transitions.

Considering the HH transitions, for the symmetric DQW [spectrum (a)] the degree of circular polarization is very small  $\mathcal{P} = 0.004 \pm 0.002$ , whereas, for the asymmetric spectra (b) and (c)  $\mathcal{P} = 0.32 \pm 0.002$  and  $\mathcal{P} = 0.055 \pm 0.002$ , respectively. By using Eq. (1), the spin-relaxation time can be estimated for each sample and is given by (a)  $\tau_s = \tau/(165 \pm 83)$ , (b)  $\tau_s = \tau/(0.56 \pm 0.01)$ , and (c)  $\tau_s = \tau/(8.0 \pm 0.3)$ . The maximum values of  $\mathcal{P}$  are obtained for sample (b). This can be understood on the basis of the relative values of the Dresselhaus and Rashba contributions to the SOC as we will discuss in the next paragraphs. Additional evidence for the physical origin of  $\mathcal{P}$  and  $\tau_s$  in sample (b) is obtained by measuring the  $\mathcal{P}$  dependence on temperature. Figure 3 shows this dependence for a laser excitation wavelength of  $\lambda = 787$  nm. Above 150 K the PL noise/signal ratio increases so much, and it is not possible to measure PL. As is expected,  $\mathcal{P}$  drops when the temperature increases.

## III. SPIN RELAXATION MECHANISMS

In intrinsic two-dimensional systems, the spin relaxation of the electrons in the conduction band is dominated by the Dyakonov-Perel mechanism [18,19]. The spin-relaxation rate is given by [18,19]

$$\frac{1}{\tau_s} = \langle \mathbf{\Omega} \cdot \mathbf{\Omega} \rangle \tau_p, \quad (2)$$

where  $\mathbf{\Omega}$  is the spin precession vector around the effective magnetic field induced by the SOC,  $\tau_s$  and  $\tau_p$  are the spin- and momentum relaxation times, respectively.

The Hamiltonian associated with the spin-orbit interaction is given by [8]

$$H_{SO} = \frac{\hbar}{2} \sigma \cdot \mathbf{\Omega}, \quad (3)$$

where  $\sigma$  is the vector of Pauli matrices and  $\mathbf{\Omega}$  is the precession frequency vector. The magnitude and direction of the precession vector depends on the electron quasimomentum  $\mathbf{k}$ . In a (001) DQW, two mechanisms induce an in-plane magnetic field and, consequently, the precession of the spin vector: the bulk inversion asymmetry (BIA) and the structure

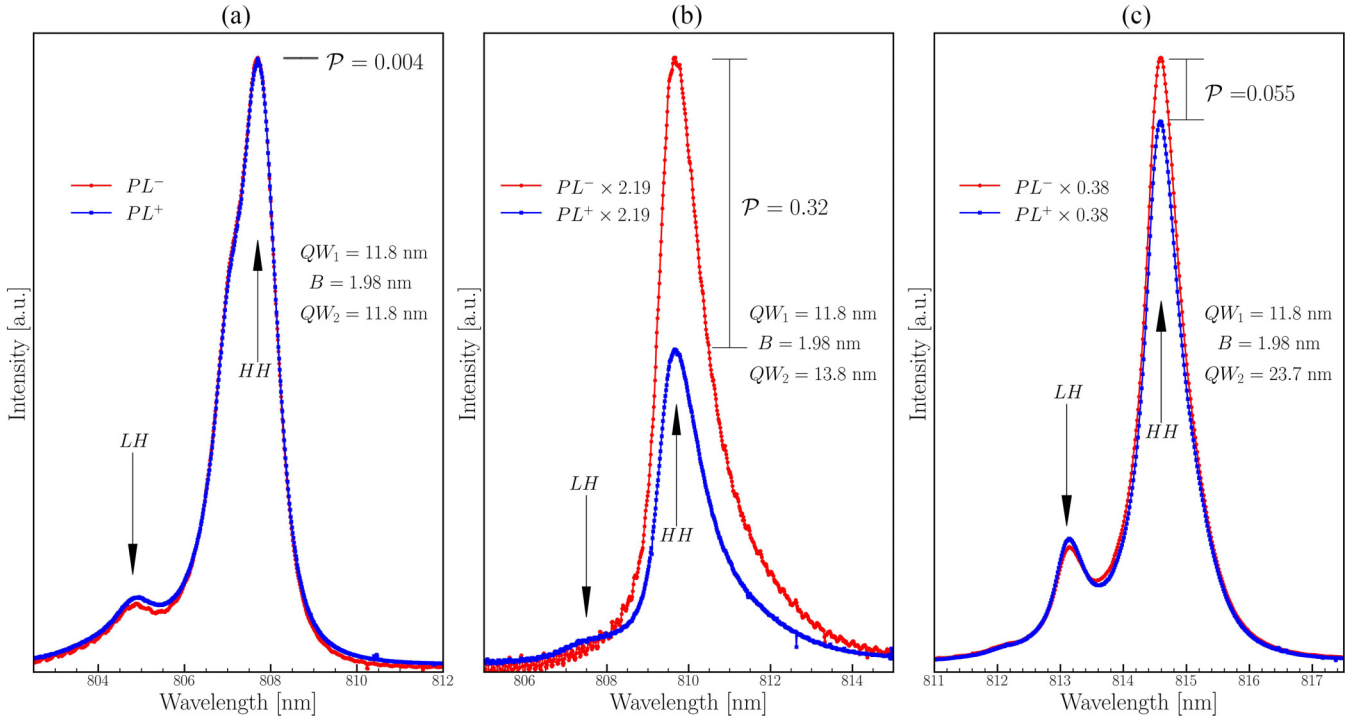


FIG. 2. PL spectra measured by exciting the sample with left circularly polarized light for (a) symmetric DQW and (b) and (c) asymmetric DQW structures. Black and red spectra correspond to left and right circularly polarized components of the PL, respectively. In the case of (a) the relaxation mechanism of the spin is dominated by the Dresselhaus effect whereas, for (b) and (c) both effects, Dresselhaus and Rashba, have important contributions to the relaxation of the electron spin. Arrows indicate the peaks corresponding to heavy- and light-hole transitions.

inversion asymmetry (SIA). The BIA component is caused by the intrinsic lack of inversion symmetry of the GaAs crystal (Dresselhaus effect). The SIA (Rashba effect) can be induced by barrier asymmetries or electric fields.

The asymmetry and the built-in electric field in the DQW structures are, in general, important to establish the relative strengths of the Dresselhaus and the Rashba effects. The contribution to the Rashba effect of the built-in electric field in our structure has been estimated by comparing the PL spectra for the asymmetric structure of Fig. 2(c) with an  $\text{Al}_{0.15}\text{Ga}_{0.85}\text{As}$  (600 nm) lower barrier of  $n$  and  $p$  types [15]. It was found that the effect of the built-in electric field is much smaller than the effect induced by the asymmetry of the DQW structure. For the  $n$ -type lower barrier of our DQW structures, a value of

$E \approx 10$  kV/cm is estimated leading to a Rashba coefficient of  $\alpha \approx 0.4 \times 10^{-4}$  eV nm [20]. However, when the laser in the PL setup illuminates the sample,  $\alpha$  is reduced since the built-in electric field is quenched by the photoexcited carrier density.

From the discussion of the last paragraph, we will consider as the major contribution to the SIA component the one associated with the break of the translation symmetry of the potential within the DQW structure. The precession vector in the DQW system can then be written as [8,19,22]

$$\begin{aligned} \Omega &= \Omega^{\text{BIA}} + \Omega^{\text{SIA}}, \\ &= \frac{\beta}{\hbar}(-k_x, k_y, 0) + \frac{\alpha}{\hbar}(k_y, -k_x, 0), \end{aligned} \quad (4)$$

where [11]

$$\begin{aligned} \beta &= \gamma \langle k_z^2 \rangle, \\ \alpha(z) &= \sum_{i=1}^4 \frac{V_{iL} - V_{iR}}{V_0} P \delta(z - z_i). \end{aligned} \quad (5)$$

In Eqs. (5),  $\gamma$  is the Dresselhaus coupling parameter,  $\langle k_z^2 \rangle$  is the squared operator  $(-i \frac{\partial}{\partial z})^2$  averaged over the conduction-band wave function,  $P$  is the interface parameter between the materials on the left (L) and right (R) sides (Al,Ga)As/GaAs interface,  $V_{iL} - V_{iR}$  is the band offset of the  $i$ th interface,  $V_0$  is the band offset of (Al,Ga)As and GaAs. The  $\delta(z - z_i)$  term indicates that the SIA is localized at the  $i$ th interface [11].

The effective SIA component of the DQW structure (more specifically, the value of  $\alpha$  in Eqs. (4)), can be obtained by averaging  $\alpha(z)$  through the DQW. This leads to  $\alpha \propto$

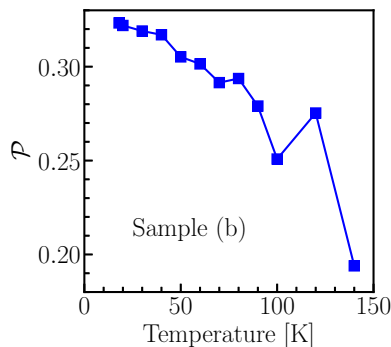


FIG. 3. Temperature dependence of the spin-polarization  $\mathcal{P}$  for the laser excitation wavelength of  $\lambda = 787$  nm. Note that the polarization drops with increasing temperature.

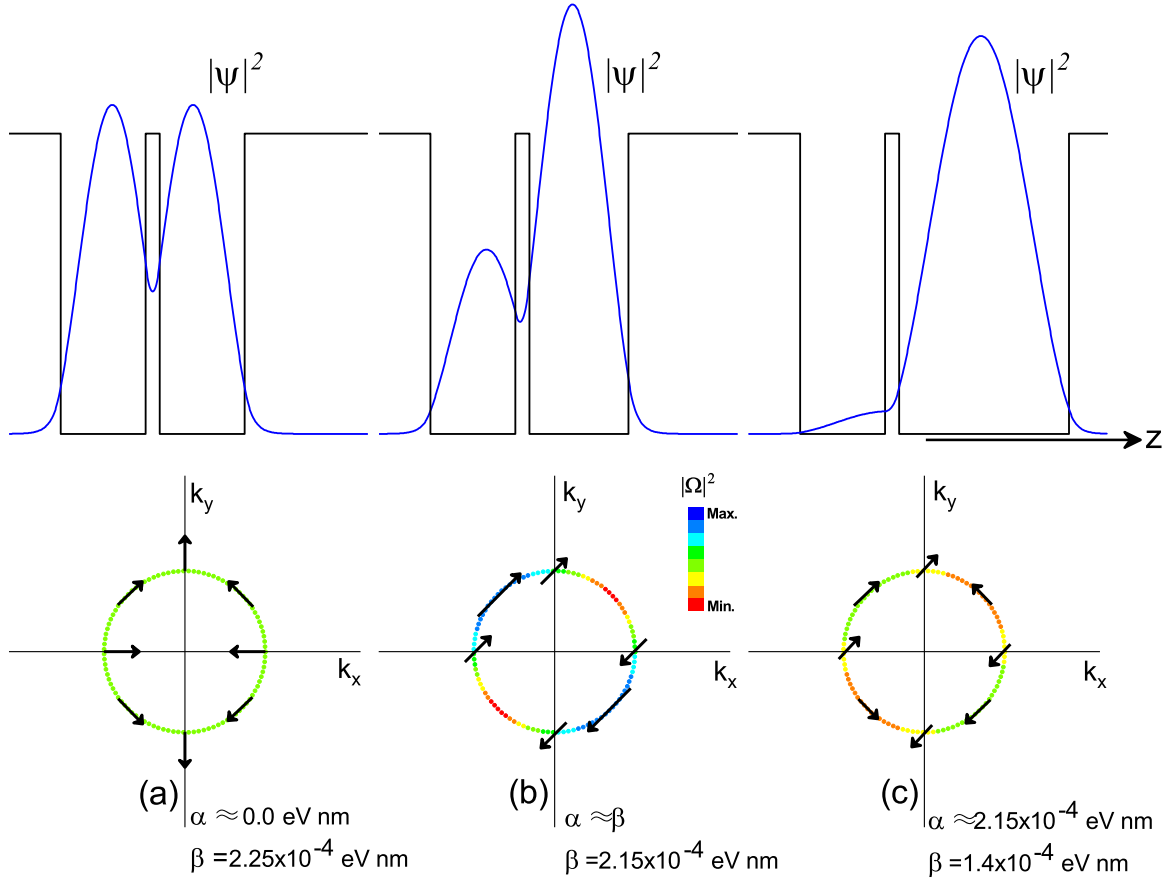


FIG. 4. Probability density ( $|\Psi|^2$ , upper diagrams) for DQWs consisting of a  $d = 11.9$ -nm-thick QW coupled to a second QW of thickness: (a)  $d = 11.9$  nm, (b)  $d = 13.8$  nm, and (c)  $d = 23.7$  nm. Below each DQW, we show the corresponding  $\Omega \cdot \Omega$  diagram in the  $k$  space. The used values of  $\alpha$  and  $\beta$  coefficients are indicated in each case. The black arrows indicate the orientation of  $\Omega$ .

$\sum_{i=1}^4 |\psi(z_i)|^2$ , i.e.,  $\alpha$  becomes proportional to the square magnitude of the electron wave function evaluated at the  $i$ th interface [11].

In polar coordinates  $(k, \phi)$ , the precession vector's square magnitude can, thus, be written as [8]

$$\Omega \cdot \Omega = \frac{k^2}{\hbar^2} (\alpha^2 + \beta^2 - 4\alpha\beta \sin \phi \cos \phi). \quad (6)$$

According to Eq. (2), the spin-relaxation time  $\tau_s$ , depends on the product of the Larmor frequency and the momentum relaxation time, i.e., large values of  $\langle \Omega \cdot \Omega \rangle \tau_p$  leads to short values of  $\tau_s$ . Thus, the spin will not relax for values of  $\langle \Omega \cdot \Omega \rangle \tau_p$  shorter than some limit. To estimate this limiting value, we can say that for the symmetric sample, this limit has been exceeded [spectrum Fig. 2(a)] and almost all spins relax. This is not the case for spectra of Figs. 2(b) and 2(c) where some spins do not relax before recombination leading to a difference in the PL strength for  $\sigma^+$  and  $\sigma^-$  polarizations. Thus, the optically excited electrons must have felt a smaller  $\langle \Omega \cdot \Omega \rangle \tau_p$  value in the conduction band.

#### IV. PERSISTENT SPIN HELIX WAVES

The condition  $\alpha = \beta$  leads to the formation of the helical spin-density waves, the called persistent spin helix (PSH) [20–22]. In this case,  $\Omega$  becomes oriented either only

along  $[110]$  or the  $[\bar{1}\bar{1}0]$  directions. In the PSH mode, the spin orientation between collisions remains coherent and the Dyakonov-Perel mechanism is completely suppressed. Along the PSH wave, the  $z$ -axis projection of the spin oscillates and the spin orientation can be detected via time and spatially resolved techniques [20,22].

Two spin decay rates are relevant for the spin lifetime  $\tau_s$ . Namely,  $T_{SO}^{-1}$  produced in the diffusive limit (Dyakonov-Perel regime) and  $T_{PSH}^{-1}$  corresponding to the longest-lived PSH mode. The decay rates are given by [20,23]

$$\begin{aligned} \frac{1}{T_{SO}} &\approx 8D_s \frac{m^{*2}}{\hbar^4} (\beta_3^2 + \alpha^2 + \beta^2), \\ \frac{1}{T_{PSH}} &\approx 2D_s \frac{m^{*2}}{\hbar^4} [3\beta_3^2 + (\alpha - \beta)^2], \end{aligned} \quad (7)$$

where  $m^*$  is the effective mass of the conduction-band electrons,  $\beta_3$  is the cubic Dresselhaus coefficient, and  $D_s$  is the spin-diffusion coefficient. The relevant times for the experiments are between  $T_{SO}$  and  $T_{PSH}$  [20,23]. Just after laser excitation (and before the PSH formation in the case of  $\alpha \approx \beta$ ), the spin-relaxation time is associated with  $T_{SO}$  (Dyakonov-Perel regime). After this time and if the PSH is formed, the spin-relaxation time approaches  $T_{PSH}$ . Considering, in general, that  $T_{PSH} \gg T_{SO}$ , thus, the formation of the PSH leads to an increase in the spin lifetime.



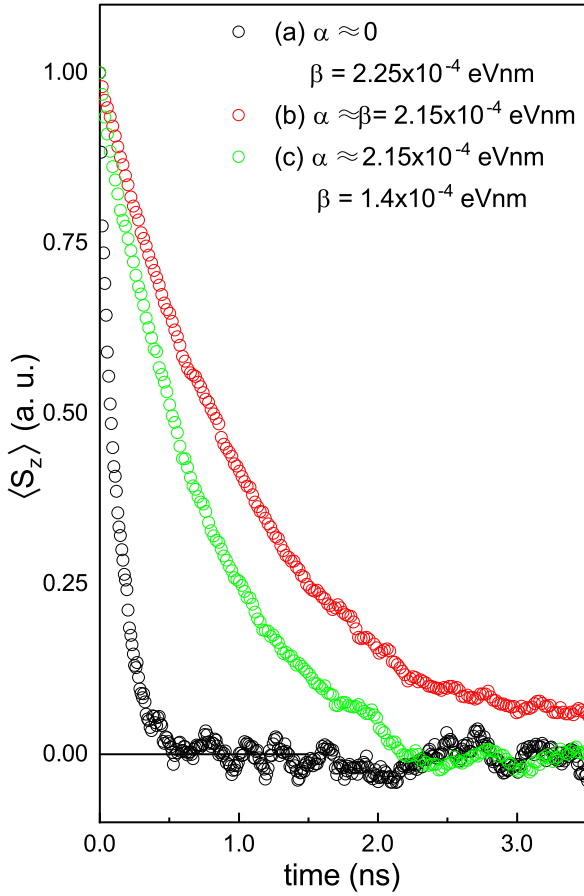


FIG. 5. Spin dynamics obtained by using Monte Carlo simulations for 1000 particles. The simulations correspond to: (black) symmetric DQW ( $d = 11.9$  nm), (red) slightly asymmetric DQW ( $d = 13.8$  nm), and (green) asymmetric DQW ( $d = 23.7$  nm). The average value of  $\langle S_z(t) \rangle$  depends strongly on  $d$ . The simulations show that the formation of the PSH plays an important role in the relaxation time of the spin. In the simulation, we have used the value  $D_s = (38 \pm 1.5) \mu\text{m}^2/\text{ns}$  [20].

As is shown in Eqs. (7), the decay rates are dependent on  $D_s$  and  $\beta$ .  $\alpha$  and  $\beta$  parameters. In a DQW system,  $D_s$  is strongly dependent on the electron density induced by doping or by photon absorption [20,23]. Values for  $D_s$  in the range of  $60\text{--}380 \text{ cm}^2/\text{s}$  for electron densities in the range of  $1.0\text{--}5.0 \times 10^{11} \text{ cm}^{-2}$  have been reported in the literature [20,23]. In the case of our samples, we take the values of  $D_s = (38 \pm 1.5) \mu\text{m}^2/\text{ns}$  and  $\beta_3 = 0.7 \times 10^{-4} \text{ eV nm}$  [20].

We estimate the values for  $\alpha$  and  $\beta$  coefficients for each sample as follows: the coefficients  $\beta$  are obtained by using Eq. (5), the value of  $\gamma = 17 \text{ meV nm}^3$  [11] and the factor  $\langle k_z^2 \rangle$  obtained from the probability density shown for each sample in Fig. 4. For the symmetric sample ( $d = 11.9$  nm) no Rashba effect is expected and, thus,  $\alpha = 0$ . Considering that for the slightly asymmetric DQW ( $d = 13.8$  nm) both mechanisms (Dresselhaus and Rashba) have important contribution, we assume  $\alpha \approx \beta$ . These values of  $\alpha$  fix the amplitude of the thickness-dependence equation of  $\alpha$  [Eq. (5)]. With this equation and the value of  $d = 23.7$  nm, we estimate  $\alpha \approx 2.0 \times 10^{-4} \text{ eV/nm}$  for the asymmetric DQW.

Figure 4 indicates for each sample the values for  $\alpha$  and  $\beta$  obtained from the experiments (as it will be detailed). By using these values a plot of  $\mathbf{\Omega} \cdot \mathbf{\Omega}$  [Eq. (6)] in  $k$  space is shown in Fig. 4. For sample (a),  $\mathbf{\Omega} \cdot \mathbf{\Omega}$  is isotropic. Arrows in Fig. 4(a) show the angular distribution of  $\mathbf{\Omega}$  in the  $k$  space. Note, that the arrows are oriented in all directions. For sample (b),  $\alpha$  and  $\beta$  become approximately equal, leading to the formation of a PSH and a maximum spin-relaxation time and a maximum anisotropy of the precession vector [Fig. 4(b)]. In this case, arrows are oriented only along  $[110]$  and  $[\bar{1}10]$ . When  $d$  increases more [Fig. 4(c)] the difference between  $\alpha$  and  $\beta$  increases reducing the anisotropy and the relaxation time.

## V. SPIN DYNAMICS AND MONTECARLO SIMULATIONS

The electrons within the QW perform a two-dimensional random walk. During the free flight between collisions, the electron's spin precesses at the Larmor frequency and after each collision the spin changes its axis of precession. In this way, after  $n$  collisions, the spin relaxes (Dyakonov-Perel mechanism). In the case of the PSH mode, the field  $\mathbf{\Omega}$  has a single direction and the spin relaxation reaches its minimum value [24]. In this mode, the cross-correlation terms  $\langle \Omega_x k_y \rangle$  and  $\langle \Omega_y k_x \rangle$  lead to the PSH mode and the increase in the spin lifetime [24].

Consider the formation of a PSH with a wave vector parallel to  $y' = [\bar{1}10]$ . Near the condition for the PSH formation ( $\alpha \approx \beta$  and  $\beta_3 \approx 0$ ), the evolution of the spin is given by the diffusion equation [24],

$$\frac{\langle S_{z,n+1} \rangle - \langle S_{z,n} \rangle}{\tau_p} = \tau_p \langle v_y^2 \rangle \left[ \frac{1}{2} \frac{\partial^2 \langle S_{z,n} \rangle}{\partial y'^2} - \frac{m^{*2}}{2\hbar^4} (\alpha + \beta)^2 \langle S_{z,n} \rangle - \frac{m^*}{\hbar^2} (\alpha + \beta) \frac{\partial \langle S_{y',n} \rangle}{\partial y'} \right], \quad (8)$$

where  $\langle S_{z,n} \rangle$  is the projection of the spin along  $z$  after the  $n$ -electron collision event, and  $\langle S_{y',n} \rangle$  is the projection of the spin along  $y'$  after the  $n$  electron collision event. The timescale is given by  $t = n\tau_p$ . The first derivative term in Eq. (8) corresponds to the cross correlation associated with the PSH formation. This term is fundamental to establish the average spin decay time. Namely, it increases the time decay of  $\langle S_z \rangle$ . In the time continuum limit (parameter  $n$  continuum), the general solutions of Eq. (8) have the form:  $\langle S_z \rangle \propto e^{-\omega t + iq'y'}$ , and  $\langle S_{y'} \rangle \propto ie^{-\omega t + iq'y'}$  where  $\omega$  and  $q'$  are the PSH frequency and wave number, respectively. By using these solutions Eq. (8) can be written as

$$\frac{d\langle S_z \rangle}{dt} \approx -\tau_p \langle v_y^2 \rangle \left[ \frac{1}{2} q'^2 + \frac{m^{*2}}{2\hbar^4} (\alpha + \beta)^2 \right] \langle S_z \rangle + \tau_p \langle v_y^2 \rangle \left[ \frac{m^*}{\hbar^2} (\alpha + \beta) q' \right] \langle S_z \rangle. \quad (9)$$

It is clear, that the first (negative) and the second (positive) terms on the right side of Eq. (9), increases and decreases  $|d\langle S_z \rangle/dt|$ , respectively. In the limit where the PSH conditions are completely fulfilled ( $\alpha = \beta$  and  $\beta_3 = 0$ ) the solution leads to  $\omega = 0$  and  $q' = 2m^*\beta/\hbar^2$ . That is, the average spin projec-

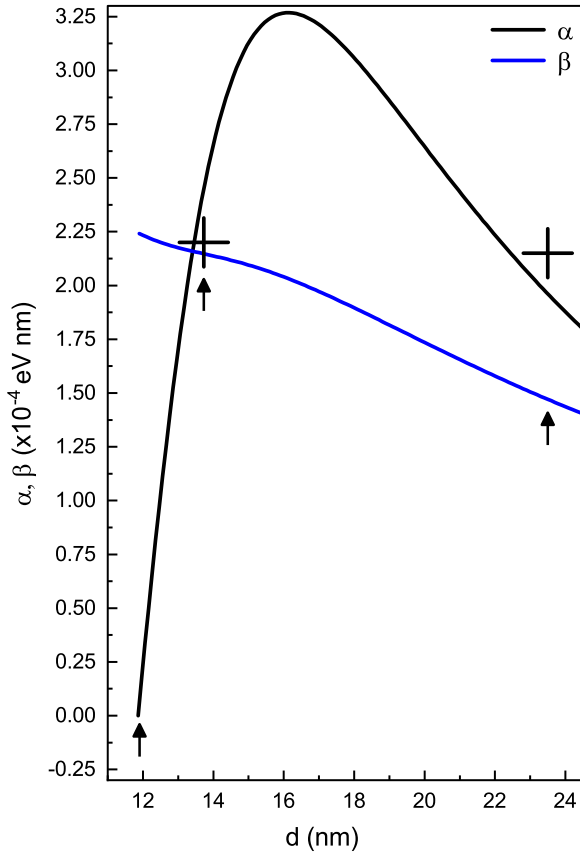


FIG. 6.  $\alpha$  and  $\beta$  coefficients as function of  $d$  calculated by using Eq. (5) and the probability density for each DQW structure. The crosses are the values for  $\alpha$  estimated experimentally (see the text for details).

tion  $\langle S_z \rangle$  becomes time independent. Otherwise, far from the PSH condition, the Dyakonov-Perel mechanism relaxes the spin. These physical mechanisms lead to the relaxation times given by Eqs. (7).

By considering the angular distribution for  $|\Omega|\tau_p$ , and the spin-diffusion mechanisms described by Eq. (9), a Monte Carlo simulation was performed to study the spin dynamics [24,25]. The values for  $\beta$  were deduced from Eqs. (5), whereas, the values for  $\alpha$  were adjusted around the values obtained from Eqs. (5). The simulations were performed assuming that the spin is initially oriented along the [001] direction. Then, 1000 electrons diffuse isotropically along the [100] and [010] directions, performing a two-dimensional random walk. For each direction, the free path for the  $n$ th collision, was determined statistically by using a Gaussian distribution normalized to the mean free path. In the simulation, the mean momentum relaxation time was estimated by using the relation  $\tau_p = 2D_s/\langle v^2 \rangle$  [23], where  $\langle v^2 \rangle$  is the average electron velocity determined from a thermal distribution [25].

Figure 5 shows the spatially averaged spin  $\langle S_z(t) \rangle$  obtained for the symmetric (black dots), slightly asymmetric (red dots), and asymmetric (green dots) DQWs. Note the huge difference in the decay time of  $\langle S_z(t) \rangle$ . The lifetime for the electrons in the conduction band in a QW system is in the range from 0.350 to 1.0 ns [26,27]. Assuming a mean lifetime approximately equal to 0.80 ns, the mean value of  $\langle S_z(t) \rangle$  is approximately equal to 0.02, 0.52 and 0.3 for the symmetric, slightly asymmetric and asymmetric DQWs, respectively. These values are in good agreement with the spin-polarization values of  $0.008 \pm 0.004$ ,  $0.64 \pm 0.004$ , and  $0.11 \pm 0.004$  estimated experimentally using  $\mathcal{P}/\mathcal{P}_0$ .

## VI. GENERAL QW THICKNESS

To capture the general behavior of the  $\alpha$  and  $\beta$  coefficients, we have simulated both of them on a function of the QW thickness  $d$ . The probability density of the electrons in the conduction band was calculated in function of  $d$ , which determines  $\Omega$ ,  $\langle k_z^2 \rangle$  and  $|\psi(z_i)|^2$ . The amplitude of simulated  $\alpha$  was scaled to fit the experimental values obtained for samples (a)–(c). Figure 6 shows the simulation results.  $\beta$  is always a decreasing function of  $d$ , whereas,  $\alpha$  has a maximum and then decreases. We indicate with vertical arrows the values corresponding to our DQWs. Note that the condition  $\alpha \approx \beta$  is closely reached in sample (b) with  $d = 14$  nm as expected. The experimental values are indicated by the crosses. The simulation gives additional evidence for the experimental values of  $\alpha$  obtained experimentally and its evolution with  $d$ .

## VII. CONCLUSIONS

To summarize, we have shown that the spin-relaxation time of electrons in the conduction band can be modulated in a DQW system. By changing the relative thicknesses of the QWs, the Larmor frequency becomes anisotropic leading to an anisotropic spin-relaxation time and the formation of PSH. To describe the spin dynamics, the Dresselhaus and Rashba effects were considered. For symmetric QWs, the Dresselhaus effect is the dominant one, whereas, for the anisotropic DQW system, the Rashba effect becomes also important. We found that the relaxation time reaches a maximum value for a DQW system with relative thicknesses of approximately 1.17 where the spin helix condition is reached with  $\alpha = \beta$ .

## ACKNOWLEDGMENTS

We thank E. Ontiveros, F. Ramírez-Jacobo, L. E. Guevara-Macías, and J. Gonzalez-Fortuna for their skillful technical support. This work was supported by Consejo Nacional de Ciencia y Tecnología (Grant No. FC 2016-02-2093).

[1] S. A. Wolf, D. D. Awschalom, R. A. Buhrman, J. M. Daughton, S. von Molnár, M. L. Roukes, A. Y. Chtchelkanova, and D. M. Treger, *Science* **294**, 1488 (2001).

[2] *Semiconductor Spintronics and Quantum Computation*, edited by D. D. Awschalom, D. Loss, and N. Samarth (Springer-Verlag, Berlin, 2002).

- [3] Y. K. Kato, R. C. Myers, A. C. Gossard, and D. D. Awschalom, *Phys. Rev. Lett.* **93**, 176601 (2004).
- [4] A. Hirohata, K. Yamada, Y. Nakatani, Ioan-Lucian Prejbeanu, B. Diény, P. Pirro, and B. Hillebrands, *J. Magn. Magn. Mater.* **509**, 166711 (2020).
- [5] S. D. Ganichev, V. V. Bel'kov, L. E. Golub, E. L. Ivchenko, P. Schneider, S. Giglberger, J. Eroms, J. De Boeck, G. Borghs, W. Wegscheider, D. Weiss, and W. Prettl, *Phys. Rev. Lett.* **92**, 256601 (2004).
- [6] G. Dresselhaus, *Phys. Rev.* **100**, 580 (1955).
- [7] J.-W. Luo, G. Bester, and A. Zunger, *Phys. Rev. Lett.* **102**, 056405 (2009).
- [8] N. S. Averkiev, L. E. Golub, A. S. Gurevich, V. P. Evtikhiev, V. P. Kochereshko, A. V. Platonov, A. S. Shkolnik, and Y. P. Efimov, *Phys. Rev. B*, **74**, 033305 (2006).
- [9] D. J. English, J. Hübner, P. S. Eldridge, D. Taylor, M. Henini, R. T. Harley, and M. Oestreich, *Phys. Rev. B*, **87**, 075304 (2013).
- [10] Y. F. Hao, Y. H. Chen, Y. Liu, and Z. G. Wang, *Europhys. Lett.* **85**, 37003 (2009).
- [11] Y.-F. Hao, *Phys. Lett. A* **379**, 2859 (2015).
- [12] D. Richards, B. Jusserand, H. Peric, and B. Etienne, *Phys. Rev. B*, **47**, 16028(R) (1993).
- [13] A. Violante, R. Hey, and P. V. Santos, *Phys. Rev. B*, **91**, 125302 (2015).
- [14] O. Ruiz-Cigarrillo, L. F. Lastras-Martínez, E. A. Cerda-Méndez, G. Flores-Rangel, C. A. Bravo-Velazquez, R. E. Balderas-Navarro, A. Lastras-Martínez, N. A. Ulloa-Castillo, K. Biermann, and P. V. Santos, *Phys. Rev. B*, **103**, 035309 (2021).
- [15] C. A. Bravo-Velázquez, L. F. Lastras-Martínez, O. Ruiz-Cigarrillo, G. Flores-Rangel, L. Estefania Tapia-Rodríguez, K. Biermann, and P. V. Santos, *Phys. Status Solidi B* **259**, 2100612 (2022).
- [16] M. I. Dyakonov and V. I. Perel, in *Optical Orientation*, edited by F. Meier and B. P. Zakharchenya (North-Holland, Amsterdam, 1984).
- [17] B. Baylac, X. Marie, T. Amand, M. Brousseau, J. Barrau, and Y. Shekun, *Surf. Sci.* **326**, 161 (1995).
- [18] M. I. Dyakonov, in *Spin Physics in Semiconductors*, edited by M. I. Dyakonov (Springer-Verlag, Berlin, 2008).
- [19] R. T. Harley, in *Spin Physics in Semiconductors*, edited by M. I. Dyakonov (Springer-Verlag, Berlin, 2008).
- [20] M. P. Walser, C. Reichl, W. Wegscheider, and G. Salis, *Nature Phys* **8**, 757 (2012).
- [21] B. Andrei Bernevig, J. Orenstein and S.-C. Zhang, *Phys. Rev. Lett.* **97**, 236601 (2006).
- [22] J. D. Koralek, C. P. Weber, J. Orenstein, B. A. Bernevig, S.-C. Zhang, S. Mack, and D. D. Awschalom, *Nature (London)* **458**, 610 (2009).
- [23] S. Anghel, A. V. Poshakinskiy, K. Schiller, G. Yusa, T. Mano, T. Noda, and M. Betz, *J. Appl. Phys.* **132**, 054301 (2022).
- [24] L. Yang, J. Orenstein and D.-H. Lee, *Phys. Rev. B*, **82**, 155324 (2010).
- [25] P. L. J. Helgers, J. A. H. Stotz, H. Sanada, Y. Kunihashi, K. Biermann, and P. V. Santos, *Nat. Commun.* **13**, 5384 (2022).
- [26] E. O. Göbel, H. Jung, J. Kuhl, and K. Ploog, *Phys. Rev. Lett.* **51**, 1588 (1983).
- [27] Y. Masumoto, S. Shionoya, and H. Kawaguchi, *Phys. Rev. B*, **29**, 2324(R) (1984).